Article

The Influence of Forced Convective Heat Transfer on Hybrid Nanofluid Flow in a Heat Exchanger with Elliptical Corrugated Tubes: Numerical Analyses and Optimization

Yacine Khetib [1,2,*], Hala M. Abo-Dief [3,*], Abdullah K. Alanazi [3], Zafar Said [4,5,*], Saim Memon [6,7,*], Suvanjan Bhattacharyya [8] and Mohsen Sharifpur [9,10,*]

1   Mechanical Engineering Department, Faculty of Engineering, King Abdulaziz University, Jeddah 80204, Saudi Arabia
2   Center of Research Excellence in Renewable Energy and Power, King Abdulaziz University, Jeddah 80204, Saudi Arabia
3   Department of Chemistry, College of Science, Taif University, P.O. Box 11099, Taif 21944, Saudi Arabia; aalanaz4@tu.edu.sa
4   Department of Sustainable and Renewable Energy Engineering, University of Sharjah, Sharjah P.O. Box 27272, United Arab Emirates
5   U.S.-Pakistan Center for Advanced Studies in Energy (USPCAS-E), National University of Sciences and Technology (NUST), Islamabad 24090, Pakistan
6   Solar Thermal Vacuum Engineering Research Group, London Centre for Energy Engineering, School of Engineering, London South Bank University, London SE1 0AA, UK
7   Department of Engineering and Technology, School of Computing and Engineering, University of Huddersfield, Huddersfield, West Yorkshire HD1 3DR, UK
8   Department of Mechanical Engineering, Birla Institute of Technology and Science Pilani, Pilani Campus, Vidhya Vihar, Rajasthan 333031, India; suvanjan.bhattacharyya@pilani.bits-pilani.ac.in
9   Department of Mechanical and Aeronautical Engineering, University of Pretoria, Pretoria 0002, South Africa
10   Department of Medical Research, China Medical University Hospital, China Medical University, Taichung 404, Taiwan
*   Correspondence: ykhetib@yahoo.com (Y.K.); h.abodeif@tu.edu.sa (H.M.A.-D.); zsaid@sharjah.ac.ae (Z.S.); S.Memon@lsbu.ac.uk (S.M.); mohsen.sharifpur@mail.cmuh.org.tw (M.S.); Tel.: +44-(0)20-7815-7510 (S.M.)

Featured Application: Cooling of Power Electronic Devices, Electromechanical Machines, Thermoelectric Devices, and Bioengineering Applications.

Abstract: The capabilities of nanofluids in boosting the heat transfer features of thermal, electrical and power electronic devices have widely been explored. The increasing need of different industries for heat exchangers with high efficiency and small dimensions has been considered by various researchers and is one of the focus topics of the present study. In the present study, forced convective heat transfer of an ethylene glycol/magnesium oxide-multiwalled carbon nanotube (EG/MgO-MWCNT) hybrid nanofluid (HNF) as single-phase flow in a heat exchanger (HE) with elliptical corrugated tubes is investigated. Three-dimensional multiphase governing equations are solved numerically using the control volume approach and a validated numerical model in good agreement with the literature. The range of Reynolds numbers (Re) 50 < Re < 1000 corresponds to laminar flow. Optimization is carried out by evaluation of various parameters to reach an optimal case with the maximum Nusselt number (Nu) and minimum pressure drop. The use of hybrid nanofluid results in a greater output temperature, a higher Nusselt number, and a bigger pressure drop, according to the findings. A similar pattern is obtained by increasing the volume fraction of nanoparticles. The results indicate that the power of the pump is increased when EG/MgO-MWCNT HNFs are employed. Furthermore, the thermal entropy generation reduces, and the frictional entropy generation increases with the volume fraction of nanoparticles and Re number. The results show that frictional and thermal entropy generations intersect by increasing the Re number, indicating that frictional entropy generation can overcome other effective parameters. This study concludes that the EG/MgO-MWCNT HNF with a volume fraction (VF) of 0.4% is proposed as the best-case scenario among all those considered.

1. Introduction

Improving the thermal energy transport coefficient in forced convection flow inside channels is an area that has long piqued the interest of heat transfer (HT) experts because of the important industrial applications of channel flows. So far, various methods have been proposed by researchers, including the use of grooves, ribs, and turbulators [1–8], as well as magnetic field and electric field [9–15]. The dimensions, type of working fluid, and arrangement of flow in the exchanger are among the important factors for the performance of heat exchangers. The replacement of conventional coolants with a suspension of metallic/nonmetallic nanoparticles in liquids is another proposed approach that has received much attention in the recent two decades. Various studies have shown that these fluids, called nanofluids (NFs), exhibit better thermal conductivity and cooling performance than conventional coolants such as water and engine oil [16–28].

The significance of the thermal and flow characteristics of nanofluids has been reported. Santra et al. [29] carried out a study focusing on the thermohydraulic characteristics of Cu-water NFs inside a plain horizontal channel by influencing the intensity of the electric field and volume fraction (VF) of nanoparticles (NPs). They discovered that when the volume percentage of NPs and the Reynolds number (Re) increase, heat flow improves. Yin et al. [30] reported a decrease in the Nusselt number (Nu) and friction factor (f) while investigating the thermohydraulic characteristics of air flow inside sinusoidal wavy corrugated channels. They carried out a numerical study by employing the phase shift between walls and reported optimal performance in the low-Re region with a phase shift of zero. Manca et al. [31] performed computational analysis of the thermal and flow performance of NF inside a ribbed duct and reported an enhancement in the Nu and pressure drop (PD) with an increase in the VF of NPs and Re. Mohammed et al. [32] also reported similar results for their numerical investigation. Heidary and Kermani [33] presented the result of thermohydraulic numerical analysis of NFs in a wavy channel. According to their findings, the Nu increases with Re, nanoparticle volume percentage, and wave amplitude. The simulated analysis by Ahmed et al. [34], employing Cu-water NF as the working fluid flowing in a triangular corrugated tube, showed an increase in HT, as well as PD, as the VF of NPs increased. In another study by Ahmed et al. [35], an enhancement in HT was reported with an increase in the Re, VF of NPs, and amplitude of the wavy wall. Furthermore, Ahmed et al. [36] investigated the flow of NF inside a trapezoidal-corrugated tube for HT and PD evaluation and reported an increase in HT and PD with the Re, amplitude of the channel, and VF of NPs. Arani et al. [37] implemented boehmite-alumina-ethylene glycol/water nanofluid as the working medium in a corrugated microchannel and revealed that the thermal and flow performance was significantly influenced by the morphology of the nanoparticles under consideration. The influence of the groove angle of the test section on the thermohydraulic characteristics was reported by Sadripor et al. [38]. They used SiO_2-water nanofluid as the working agent. The grooves angles were discovered to have an important influence on the performance of the corrugated duct. Hung [39] investigated Cu-water NF fluid flow and HT in a microchannel. They considered the impact of various factors on temperature distribution and showed that HT performance differs when viscous dissipation is taken into account. Torii et al. [40] carried out an experimental assessment and revealed that nanofluid performed best when data were compared with base fluids. They observed that when aggregation and particle size increase, heat transfer decreases. Mohammed et al. [41] examined several types of nanoparticles in a computational study of heat exchanger microchannels. For all types of nanofluids, they found an improvement in thermal performance and pressure drop.

It is believed that building a heat transmission device only based on the first law of thermodynamics would be inefficient, and that the second law of thermodynamics must also be taken into account when developing heat transfer devices. The second law of thermodynamics states that the design of a system must be such that it entails the lowest possible rate of entropy production. A review of the literature indicates that the analysis of forced heat transfer through channels using the second law has rarely been performed. Asha and Deepa [42] carried out an analysis in a tapered irregular channel to evaluate the entropy production of magnetomicropolar fluid with thermal radiation. Entropy production decreased when the magnetic parameter and thermal radiation parameters increased. The effect of geometrical factors on entropy production in cross-wavy channels was explored by Shi et al. [43]. Their findings indicate that heat transport is a primary cause of entropy production in the geometry under consideration. Gul et al. [44] investigated entropy production in a vertical tube with mixed convection Poiseuille flow of molybdenum disulfide Jeffrey NF. The results indicated that when the temperature decreases and the Brickman number increases, entropy production increases. Dormohammadi et al. [45] studied the entropy generation features of NF flow in sinusoidal wavy channels numerically and discovered that the lowest entropy production rate decreases as the Richardson number increases. CuO-water NF flow over a heat source inside a conduit with abrupt extension and shrinkage was studied by Nouri et al. [46]. The entropy generation number increases when the NF concentration and surface temperature of the heat source increases, whereas it decreases when the blockage ratio is increased. It is pertinent to mention that the geometry of tubes (twisted and straight), flow direction (countercurrent and concurrent), and flow rates that impact the Re numbers are critical to the performance of heat exchangers [46]. It was also found that the thermophysical properties of nanofluids, such as specific heat, viscosity, thermal conductivity, and heat transfer coefficient, are of great importance for heat transfer application in heat exchangers [47]. In addition, a recent study found that flow rate in the tube side and shell side are both critical to the performance of heat exchangers [48].

Together, these studies show that the use of nanoparticles generally increases the pressure drop (up to about 17%) and increases the heat transfer rate (up to about 28%) [32–34]. While the pressure drop is actually generally increased by the presence of nanoparticles, the effects on the heat transfer rate depend, among other factors, on the flow regime. Frequently, negative effects are observed for turbulent flow, while more promising results are obtained for laminar flow. Performing two-phase simulations can report results closer to the experimental results. Of course, this behavior is not the same in all studies, and some contradictory results have been presented.

To the best of our knowledge, no study has been performed to date on the modeling and simulation of the hydrothermal characteristics and entropy production of single-phase hybrid nanofluid (HNF) flow within a heat exchanger (HE) with elliptical corrugated tubes, based on a review of the literature. The current study was conducted in order to fill this research gap.

2. Materials and Methods

2.1. Numerical Model Methodology

Figure 1a shows a schematic of a HE with elliptical corrugated tubes and its geometrical parameters. Figure 1b illustrates a schematic of the elliptical tube considered for the present study. All boundary conditions are illustrated in Figure 1b. Figure 1c presents a detailed image of the HE with elliptical corrugated tubes studied in this paper.

(**a**)

(**b**)

(**c**)
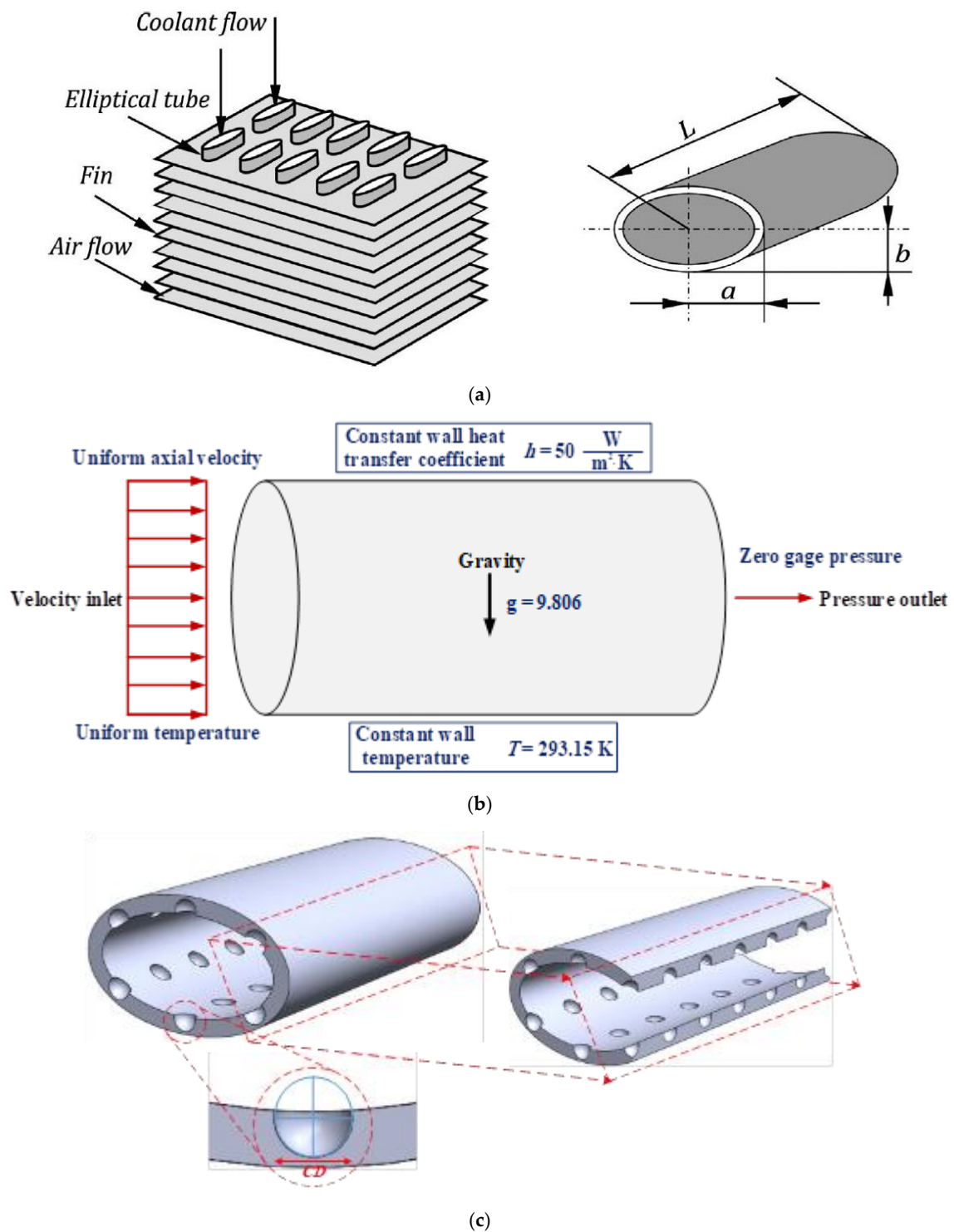
Figure 1. Schematic of (**a**) heat exchanger with elliptical corrugated tubes, (**b**) elliptical tube and boundary conditions, and (**c**) elliptical corrugated tube.

The following assumptions are considered to perform the required simulations:

- The flow is in the steady state [49].
- The ethylene glycol/magnesium oxide-multiwalled carbon nanotube (EG/MgO-MWCNT) hybrid nanofluid is simulated as a single-phase fluid.
- Laminar flow regime ($50 \leq \text{Re} \leq 1000$), $T_{wall} = 400$ K, and $T_{in} = 313$ K and 323 K.
- The convergence criterion is considered to be less than 10^{-6} for all the effective variables.
- Gravity effects and kinetic losses are considered.

- Velocity inlet and constant inlet temperature boundary conditions are used for the inlet.
- The pressure outlet boundary condition is employed for the heat exchanger exit.
- The constant temperature boundary condition is used on the side walls.
- The diffusion terms in the energy and momentum equations are approximated using second-order central difference.
- For the convective terms, the second-order upwind scheme is employed.

The governing equations for two-phase NF flow and HT in the microchannel are as follows [50–54]:

Continuity equation:

$$\nabla \cdot \left(\rho_{nf} \, V_m \right) = 0 \tag{1}$$

where ρ_{nf} is the NF density and V_m is the mean velocity.

Momentum equation:

$$\nabla \cdot \left(\rho_{nf} \, V_m V_m \right) = -\nabla P + \nabla \cdot \left(\mu_{nf} \nabla V_m \right) + (M \cdot \nabla) \cdot B \tag{2}$$

where μ_{nf} is the NF viscosity.

Energy equation:

$$\nabla \cdot \left(\rho_{nf} \, c \, V_m \, T \right) = \nabla \cdot \left(k_{nf} \, \nabla \, T \right) + \mu_0 (M \cdot \nabla) \cdot H \tag{3}$$

Table 1 shows the geometrical parameters of the heat exchanger with elliptical corrugated tubes implemented in the present investigation. The average Nu and thermal resistance coefficient for elliptical and circular tubes are presented in Table 2. Table 3 presents the required coefficients to calculate the equations of Table 1 in terms of the Nusselt number at different weight concentrations. Table 4 shows the required coefficients to calculate the equations of Table 1 in terms of the thermal resistance coefficient at different weight concentrations. The thermophysical properties of the EG/MgO-MWCNT hybrid nanofluid are presented in Table 5. In Table 6, thermal and hydrodynamic equations are given to evaluate the different effective parameters. Table 7 presents material properties, and Table 8 illustrates the thermophysical objects of the NF considered in this paper.

Table 1. Geometrical parameters.

Parameter	Value
Minor axis, b	0.73 mm
Major axis, a	1.42 mm
Corrugation diameter, CD	0.04 mm
Hydraulic diameter, $D_h = 4A/P$	1.25 mm
Length, L	500 m

Table 2. Average Nu and thermal resistance coefficient equations for elliptical (semicircular) and circular tube [54,55].

Elliptical Tube	Circular Tube
Nu	
$Nu = A' + B'Re$ (4)	$Nu = A + BRe + CRe^2$ (5)
Thermal resistance coefficient	
$\ln(100f) = a' + b' \ln Re + c'(\ln Re)^2$ (6)	$\ln(100f) = w + r \ln Re + z(\ln Re)^2$ (7)

Table 3. Coefficients required to solve equations of Table 2 in terms of Nusselt number at different weight concentrations [54,55].

Weight Concentrations (%)				Needed Coefficients
0.5	0.3	0.1	0.0	
-17.43407	-17.57942	-19.76301	-7.79878	A
0.0144	0.01414	0.0144	0.01062	B
$-3.25993 \cdot 10^{-7}$	$-3.19072 \cdot 10^{-7}$	$-3.38791 \cdot 10^{-7}$	$-1.66817 \cdot 10^{-7}$	C
13.82789	11.97992	10.8056	8.28254	A'
0.00976	0.00939	0.00902	0.00771	B'

Table 4. Coefficients required to solve equations of Table 2 in terms of thermal resistance coefficient at different weight concentrations [54,55].

Friction Coefficients	Needed Coefficients
3.22392	w
-0.19754	r
-0.0029	z
-22.3152	a'
5.72631	b'
-0.34101	c'

Table 5. Implemented thermophysical properties of hybrid nanofluid in the model [54,55].

Equation	Eq. No.
$\rho_{hnf} = (1 - \phi)\rho_{bf} + \phi\left(\rho_{MgO+MWCNT}\right)$	(8)
$c_{p,hnf} = (1 - \phi)c_{p,bf} + \phi\left(c_{p,MgO+MWCNT}\right)$	(9)
$k_{hnf} = k_{bf}\left(0.8341 + 1.1\phi^{0.243}T^{-0.289}\right)$	(10)
$\mu_{hnf} = \mu_{bf}\left[0.191\phi + 0.240\left(T^{-0.342}\phi^{-0.473}\right)\right]\exp\left(1.45T^{0.120}\phi^{0.158}\right)$	(11)
$\phi = \dfrac{\left(\frac{m}{\rho}\right)_{MgO} + \left(\frac{m}{\rho}\right)_{MWCNT}}{\left(\frac{m}{\rho}\right)_{MgO} + \left(\frac{m}{\rho}\right)_{MWCNT} + \left(\frac{m}{\rho}\right)_{EG}}$	(12)

Table 6. Implemented thermal hydrodynamic equations in the model [54,55].

Equation	Eq. No.
$\dot{Q} = \dot{m}c_p(T_{in} - T_{out})$	(13)
$h = \dfrac{\dot{Q}}{A_e \Delta T_m} = \dfrac{\dot{m}c_p(T_{in} - T_{out})}{A_e\left(\dfrac{(T_w - T_{in}) - (T_w - T_{out})}{\ln \frac{T_w - T_{in}}{T_w - T_{out}}}\right)}$	(14)
$A_e = 2\pi L\sqrt{\dfrac{a^2 + b^2}{2}}$	(15)
$Nu = \dfrac{hD_h}{k}$	(16)
$\dot{W} = \dfrac{\dot{m}\Delta P}{\rho}$	(17)
$f = \dfrac{2\Delta P D_h}{\rho U^2 L}$	(18)
$\dot{S}_{gen} = \dot{S}_{gen,T} + \dot{S}_{gen,F}$	(19)
$\dot{S}_{gen,T} = \dfrac{\dot{Q}^2}{Nu\pi k T_{in}T_{out}L}$	(20)
$\dot{S}_{gen,F} = \dfrac{8f\dot{m}^3 L}{\rho^2 \pi^2 D_h^5(T_{out} - T_{in})}\ln\dfrac{T_{out}}{T_{in}}$	(21)
$\psi = \dfrac{\dot{S}_{gen}}{\dot{m}c_p} = \dfrac{\Delta T \dot{S}_{gen}}{\dot{Q}}$	(22)

Table 7. Material properties [56].

Parameter	Value		
	Ethylene Glycol (EG)	Multiwalled Carbon Nanotubes	Magnesium Oxide Nanoparticles
Chemical Formula/Symbol	$C_2H_6O_2$	COOH-Functionalized MWCNTs	MgO
Molar mass	62.07 (g/mol)		40.30 (g/mol)
Appearance	Clear, colorless liquid	Black	White
Odor	Odorless	-	-
Density	1113.2 (kg/m^3)	~2100 (kg/m^3)	3580 (kg/m^3)
Specific heat capacity	2470 (J/kg·K)	630 (W/m·K)	964 (W/m·K)
Melting point	−12.9 (°C)	-	-
Boiling point	197.3 (°C)	-	-
Thermal conductivity (@20 °C)	0.244 (W/m·K)	50 (W/m·K)	45 (W/m·K)
Viscosity (@20 °C)	0.016 (Pa.s)	-	-
Purity	-	>97%	>99%
Content of –COOH	-	2.56 (wt%)	
Outer diameter	-	5–15 (nm)	40 (nm)
Inner diameter	-	3–5 (nm)	-
Length	-	~50 (μm)	-
SSA	-	>233 (m^2/g)	~25 (m^2/g)
Morphology	-	-	polyhedral

2.2. Validation of Numerical Model

2.2.1. Grid Study

A three-dimensional schematic of the computational domain and grid used for single-phase NF flow are presented in Figure 2. A nonuniform structured grid is employed for the HE with elliptical corrugated tubes. The grid is refined near the heat transfer walls ($y^+ \leq 1$) to capture the thickness of the viscous sublayer in the considered Re range. As shown in Figure 3, various grid resolutions are used to inspect the impact of grid sizes on the outcomes. Three grid resolutions of 3,243,983 (Grid I), 3,728,623 (Grid II) and 3,954,131 (Grid III)) are generated. By comparing the outcomes, it was decided that the grid resolution of 3,728,623 is sufficient to obtain reasonable outcomes with a maximum deviation of 0.01% for simulation time.
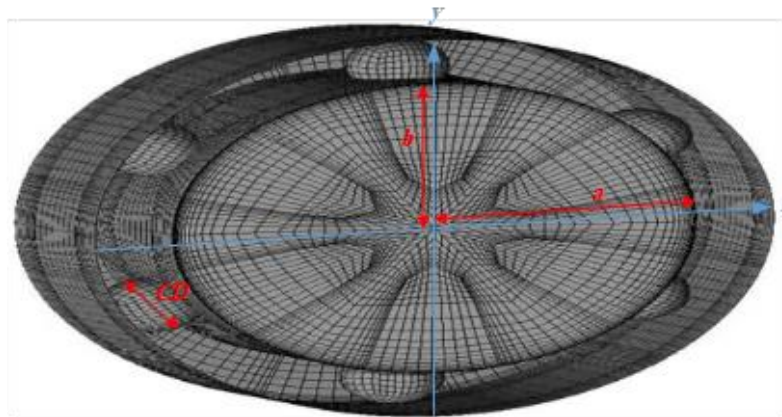
Figure 2. Schematic of computational domain and grid used in the simulations.

2.2.2. Validation Results

In this section, the computer code is verified by comparing the computational outcomes obtained from the present simulations, analytical results of Cengel [56], and numerical results of Huminic and Huminic [57], considering similar geometrical dimensions and boundary conditions. Huminic and Huminic [57] investigated the consequence of HNFs on the performance of a smooth elliptical tube using a single-phase model numerically. Figure 4 compares the analytical and numerical results. As can be seen from Figure 4, there is an excellent agreement between the analytical and numerical data [56,57] and the numerical data obtained from the present study. The maximum deviation is 1.14% in terms of the average friction factor for different Reynolds numbers.

(**a**)

(**b**)
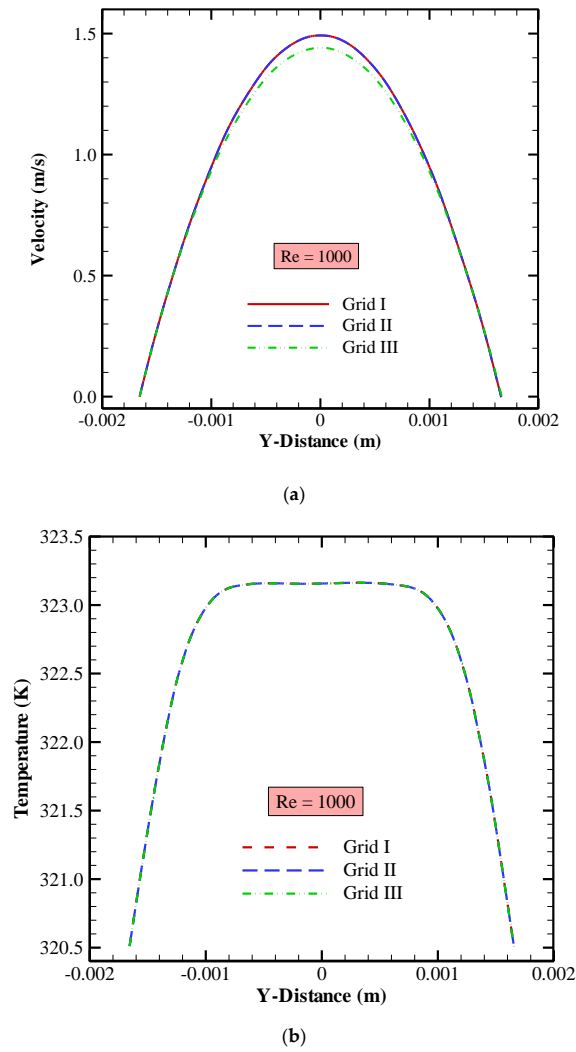
Figure 3. Grid independence test in terms of (**a**) local velocity and (**b**) local temperature.
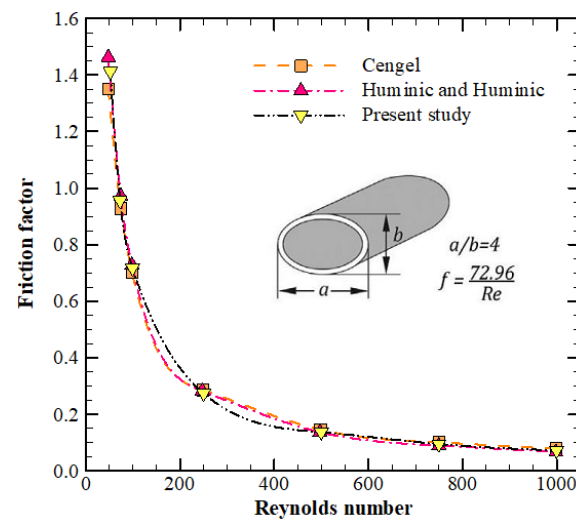
Figure 4. Average friction factor versus Reynolds number: comparison between the present results and those reported by Cengel [56] and Huminic and Huminic [57].

Table 8. Nanofluid thermophysical properties [57].

Temperature		313 K				323 K		
ϕ	EG	0.1%	0.2%	0.4%	EG	0.1%	0.2%	0.4%
k (W/m K)	0.255	0.270	0.284	0.294	0.258	0.273	0.286	0.296
μ (Pa · s)	0.0102	0.0095	0.01005	0.0111	0.00745	0.0075	0.00755	0.0088

3. Results and Discussions

In this section, the computational results are presented in terms of average Nu, HT coefficient, pumping power, PD, and entropy generation. The most appropriate case with maximum thermohydraulic performance is determined based on the second law analysis. One of the main objects of this study is to achieve the optimum volume fraction of nanoparticles using a two-phase model instead of a common single-phase model.

3.1. The Influence of Temperature and Velocity Contours on Hybrid Nanofluid Flow

Figure 5 shows the temperature and velocity contours of hybrid nanofluid flow with VF of 0.4% at Re = 1000 and inlet temperature T_{in} = 323 K. Figure 5 shows that the corrugations make local breaks in the laminar sublayer and form local vortices, leading to an augmentation in the thermal characteristics of HNF flow within the elliptical channel.
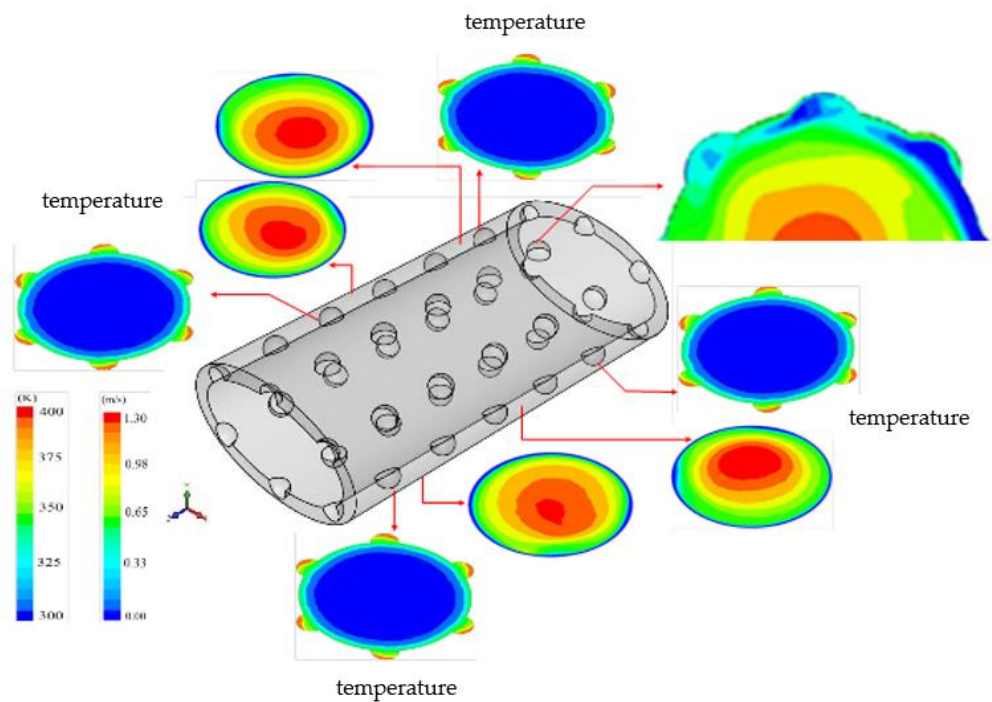
Figure 5. Temperature and velocity contours of hybrid nanofluid flow with VF of 0.4% at Re = 1000 and inlet temperature T_{in} = 323 K.

3.2. The Influence of Using Hybrid Nanofluid with Volume Fractions on Convective Heat Transfer at Various Reynold Numbers and Inlet Temperatures

Figure 6 displays the outcome of the HNF with different VF on the convective HT coefficient for various Re and inlet temperature T = 313 K. For a given Re, the HT coefficient increases with increasing nanoparticle volume fraction, while the pure base fluid HT is between those at 0.1% and 0.2% VF. Fluid flow velocity increases with the Re, disturbing the flow and increasing the heat transfer rate. At Re = 1000, the maximum heat transfer coefficient, 2700 W/m^{2}K, is achieved when the volume fraction of the EG/MgO-MWCNT nanofluid is 0.4%. The maximum value of the HT coefficient for a given Re corresponds to volume fractions of 0.4%, 0.2%, pure base fluid, and 0.1%, respectively.
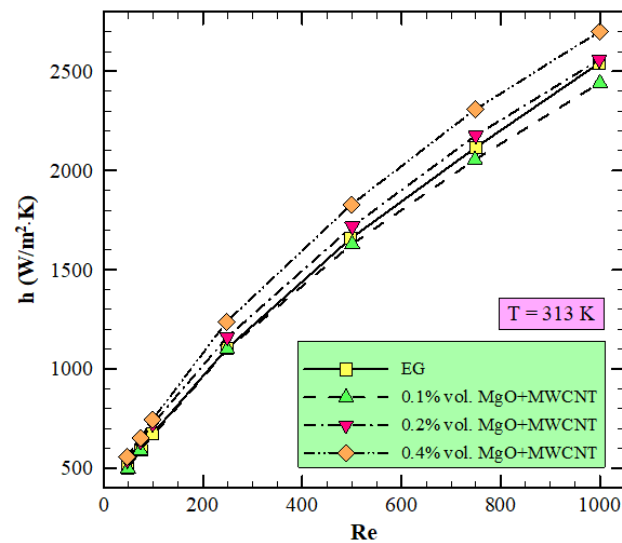
Figure 6. Effects of using HNF with different VF on HT coefficient for various Re and inlet temperature T = 313 K.

Figure 7 shows the influence of the HNF with different VF on the convective HT coefficient for various Re and inlet temperature T = 323 K. The ethylene glycol (EG) is considered the baseline. It is found that as Re increases, the average HT coefficient increases. Fluid flow velocity increases with the Re, disturbing the flow and increasing the HT rate. At Re = 1000, the maximum HT coefficient, 2480 W/m²K, is achieved when the volume fraction of the EG/MgO-MWCNT nanofluid is 0.4%. The maximum value of HT coefficient for a given Re corresponds to volume fractions of 0.4%, 0.2%, 0.1%, and pure base fluid, respectively.
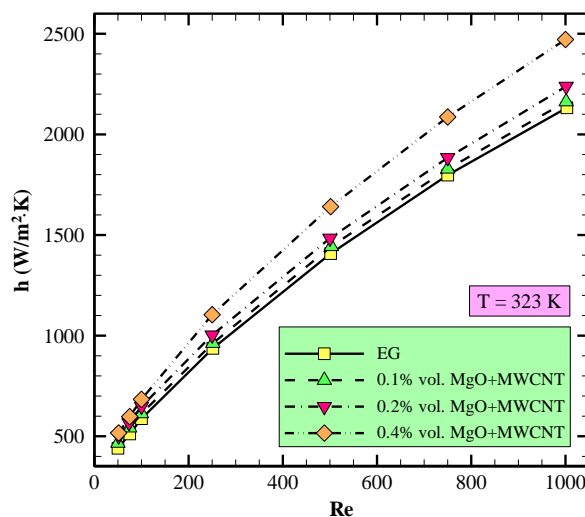
Figure 7. Influence of using HNF with different VF on HT coefficient for various Re and inlet temperature T = 323 K.

3.3. The Influence of Using Hybrid Nanofluid with Volume Fractions on the Ratio of Convective Heat Transfer to Base Fluid at Various Reynold Numbers and Inlet Temperatures

Figure 8 presents the influence of the HNF with various VF on the ratio of the convective HT coefficient of the NF to that of the base fluid for various Re and inlet temperature T = 313 K. This figure shows that the use of the EG/MgO-MWCNT HNF with a volume fraction of 0.1% is reasonable at low Re. However, at high Re, the use of the EG is more efficient than that of the EG/MgO-MWCNT HNF with a volume fraction of 0.1%. It can be demonstrated that the use of the EG/MgO-MWCNT HNF volume fractions of 2% and 0.4% is more appropriate compared to the base fluid for all Re.
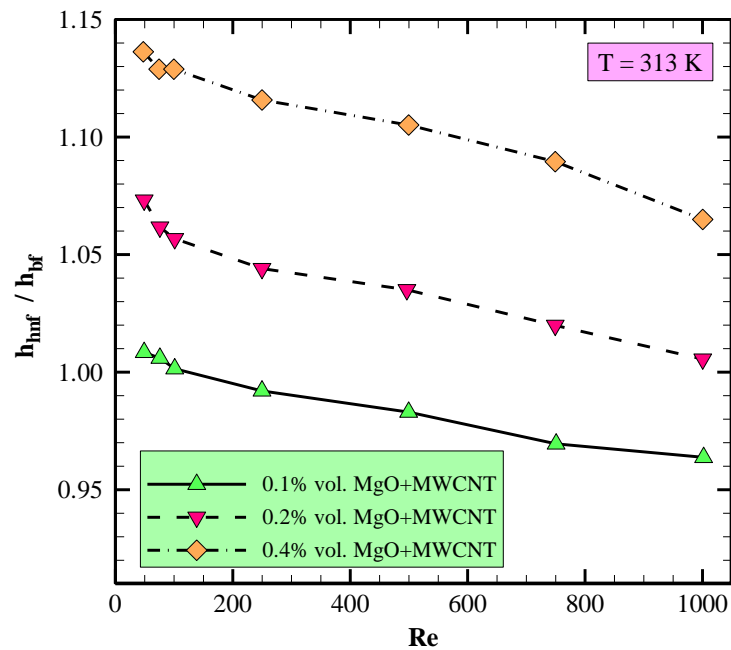
Figure 8. Influence of using HNF with different VF on HT coefficient for various Re and inlet temperature *T* = 313 K.

Figure 9 presents the influence of the HNF with various VF on the convective HT coefficient for various Reynolds numbers and inlet temperature *T* = 323 K. It is observed that the use of the EG/MgO-MWCNT HNF with volume fractions of 0.1%, 0.2%, and 0.4% is more efficient than using the base fluid (EG) for all Re. Figure 10 exemplifies the effect of the HNF with different VF on the ratio of the averaged Nu of the HNF and that of the base fluid for different Re and inlet temperature *T* = 313 K. This figure demonstrates that the use of NF at *T* = 313 K leads to minimum Nu in comparison with the base fluid.
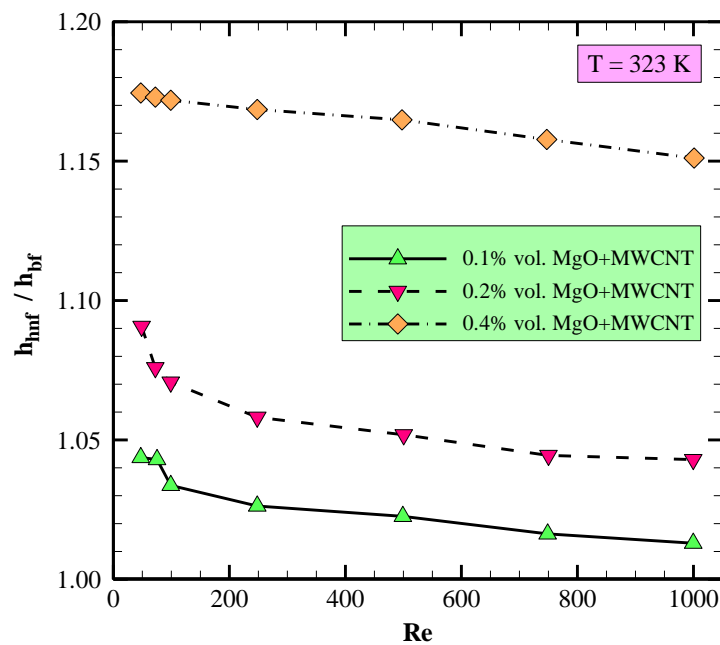
Figure 9. Influence of using HNF with different volume fractions on HT coefficient for various Re and inlet temperature *T* = 323 K.
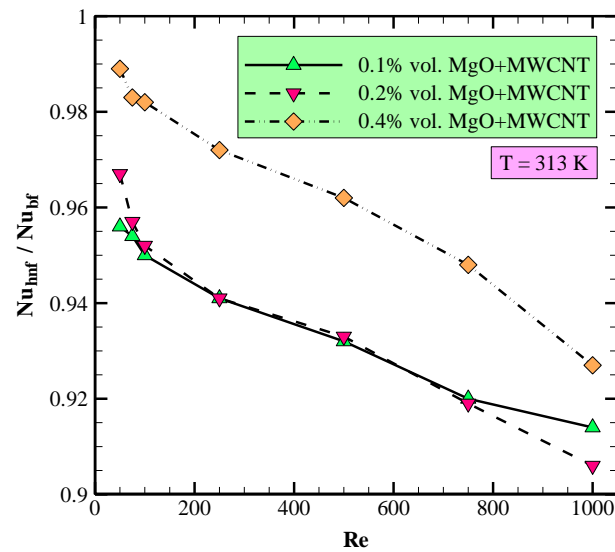
Figure 10. Effects of HNF with different VF on average Nu ratio for different Re and inlet temperature T = 313 K.

3.4. The Effects of Hybrid Nanofluid with Different Volume Fractions on Average Nu Ratio at Various Re and Selected Inlet Temperature

Figure 10 shows the effect of the HNF with different VF on the ratio of the averaged Nu of the HNF and that of the base fluid for different Re and inlet temperature T = 323 K. It is shown that the use of the EG/MgO-MWCNT HNF with a volume fraction of 0.4% at T = 323 K leads to maximum Nu in comparison with the base fluid for all Re. It is also revealed that at T = 323 K, the use of the EG/MgO-MWCNT HNF with volume fractions of 0.1% and 0.2% is efficient only at a very low Re.

Figure 11 shows the influence of the HNF with a VF of 0.4% on the Nusselt ratio due to NF flow and pure flow for various Re and inlet temperatures T = 313 K and 323 K. It is found that higher temperatures lead to higher Nusselt ratios. The Nusselt ratio is about 1.365 and 1.181 at T = 323 K and T = 313 K, respectively. The Nusselt ratio decreases slightly with the Re. Fluid flow velocity increases with the Re, disturbing the flow and increasing the HT rate.
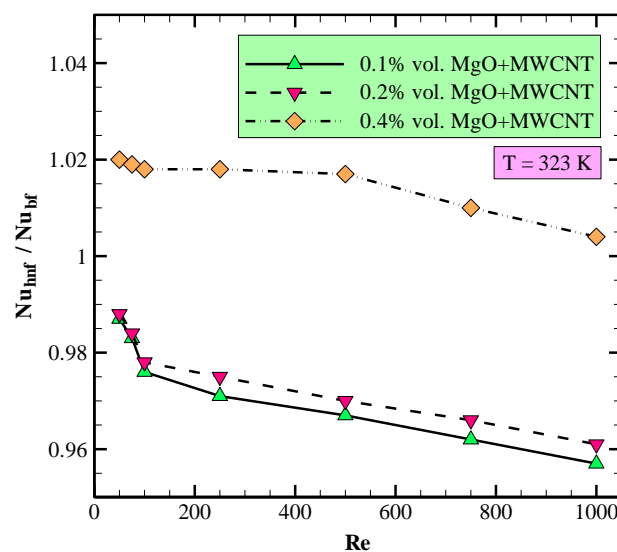
Figure 11. Effects of HNF with different VF on average Nu ratio for different Re and inlet temperature T = 323 K.

3.5. The Effects of Hybrid Nanofluid with Various Volume Fractions on Hydraulic Power at Various Re and Selected Inlet Temperature

Figure 12 shows the effect of hybrid nanofluid with various volume fractions on hydraulic power for different Re and inlet temperature T = 313 K. It is found that as the Re increases, the pumping power enhances. Fluid flow velocity increases with the Re, disturbing the flow and increasing the HT rate. The use of the EG/MgO-MWCNT HNF with a volume fraction of 4% leads to a higher pumping power compared to the other investigated cases for all Re.

Figure 13 shows the result of the HNF with various volume fractions on hydraulic power for different Re and inlet temperature T = 323 K. It is shown that the pumping power enhances with the Re. The use of the EG/MgO-MWCNT HNF with a volume fraction of 0.4% leads to higher pumping power in comparison with volume fractions of 0.1% and 0.2% for all Re.
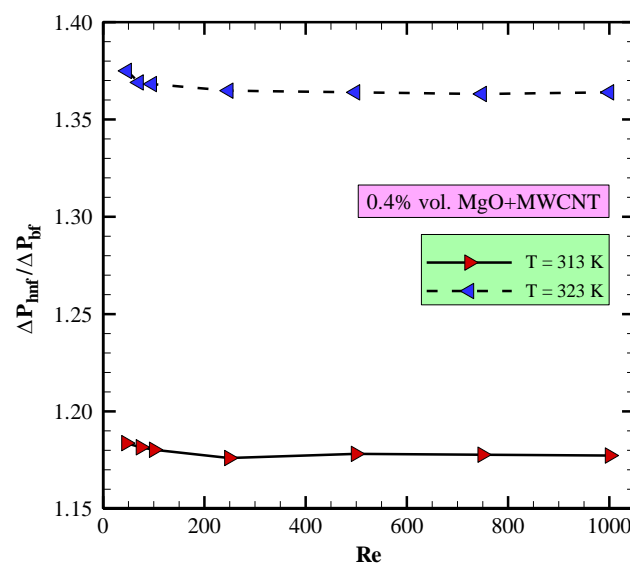
Figure 12. Effects of HNF with volume fraction of 0.4% on PD ratio for different Re and inlet temperature T = 313 K and 323 K.
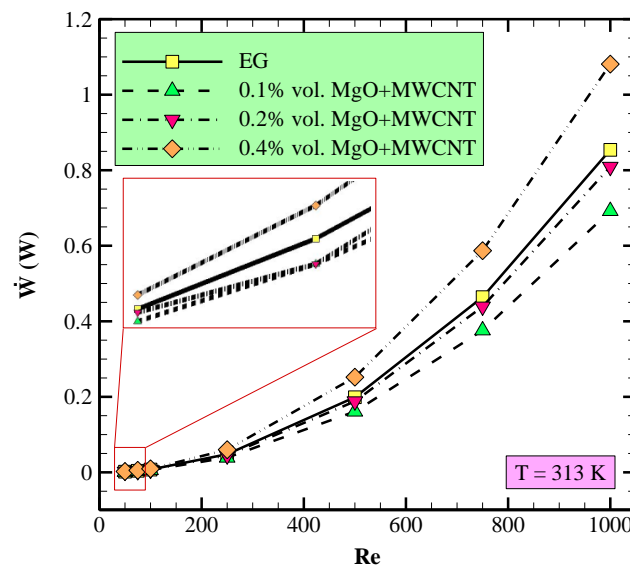
Figure 13. Influence of HNF with different VF on hydraulic power for different Re and inlet temperature T = 313 K.

Figure 14 illustrates the effect of the HNF with different VF on PD for various Re and inlet temperatures T = 313 K and T = 323 K. It is concluded that higher temperatures lead to larger PD. The use of the EG/MgO-MWCNT NF with a VF of 0.4% leads to less PD in compression with the other VF. Therefore, EG/MgO-MWCNT NF with a VF of 0.4% is introduced as the optimum case among all studied ones.
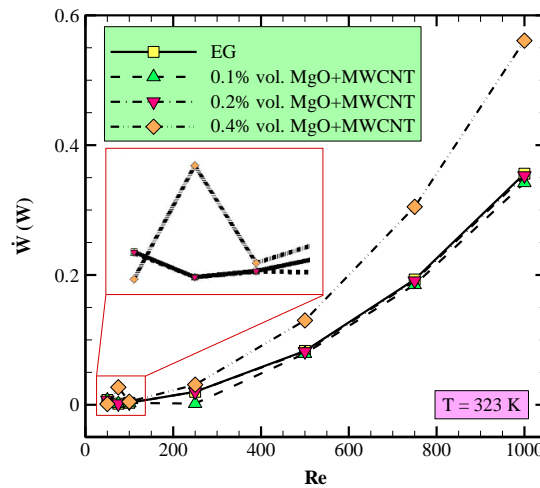
Figure 14. Influence of HNF with different VF on hydraulic power for different Re and inlet temperature T = 323 K.

3.6. The Effects of Hybrid Nanofluid with Various Volume Fractions on Pressure Reduction on Thermal Entropy Generation at Various Re and Selected Inlet Temperature

Figure 15 presents the effect of the HNF with various VF on % pressure reduction (PR) percentages on thermal entropy generation for various Re and inlet temperatures (a) T = 313 K and (b) T = 323 K. As can be seen in these figures, with an increasing Reynolds number, no significant change in pressure drop values occurs at the studied temperatures.
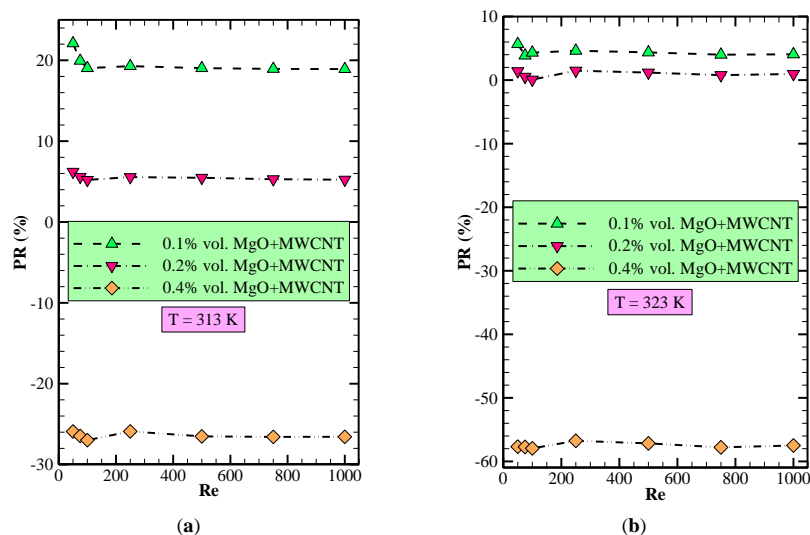
Figure 15. Effects of HNF with different VF on pressure reduction for different Re and inlet temperatures (**a**) T = 313 K and (**b**) T = 323 K.

Figure 16 illustrates the effect of hybrid nanofluid with different volume fractions on entropy generation for various Reynolds numbers and inlet temperatures T = 313 K and T = 323 K. Thermal entropy generation $\dot{S}_{gen,T}$ and frictional entropy generation $\dot{S}_{gen,F}$ are demonstrated in Figures 16 and 17. They are due to irreversibility. As shown in Figure 16a,b, thermal entropy generation decreases, and frictional entropy generation increases with the

VF of NPs and Re. It must be noted that frictional entropy generation is approximately zero at low flow velocities for both inlet temperatures. It is found that the diagrams of frictional and thermal entropy generations have an intersection, indicating the frictional entropy generation can overcome other effective parameters. The irreversibility due to HT leads to the generation of thermal entropy. Therefore, the variation in $\dot{S}_{gen,T}$ is more important at low Re. In addition, the changes in $\dot{S}_{gen,F}$ which describe the frictional irreversibility are more important at high Re, because the fluid friction in flow fields enhances with the Re. Figure 17a reveals that the values of frictional entropy generation of the EG/MgO-MWCNT HNF with a volume fraction of 0.4% are very close to those of the base fluid. However, the values of frictional entropy generation of the EG/MgO-MWCNT HNF with a VF of 0.2% are superior compared to the base fluid. Frictional entropy generation increases with the Re for both volume fractions of 0.2% and 4%. This is due to an increase in the velocity gradients and consequently an enhancement of viscous forces. Figure 17b shows that the values of frictional entropy generation for hybrid nanofluid with volume fractions of 0.1% and 0.2% are very close to that for the base fluid. Frictional entropy generation for HNF with a VF of 0.4% is more than that for ethylene glycol.

(a)

(b)
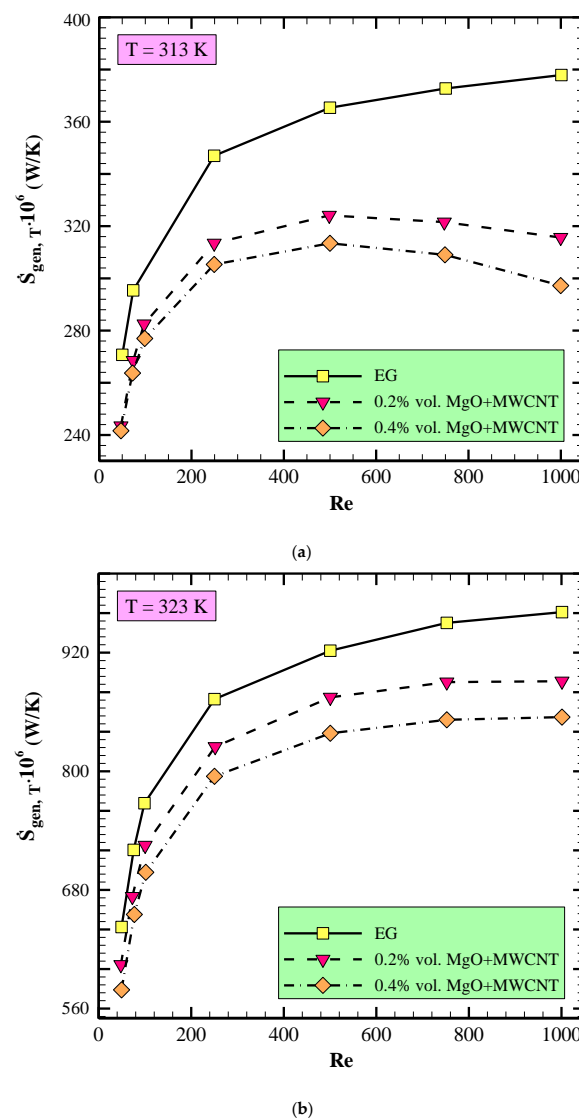
Figure 16. Effects of HNF with different VF on thermal entropy generation for different Re and inlet temperatures of (**a**) *T* = 313 K and (**b**) *T* = 323 K.

(**a**)

(**b**)
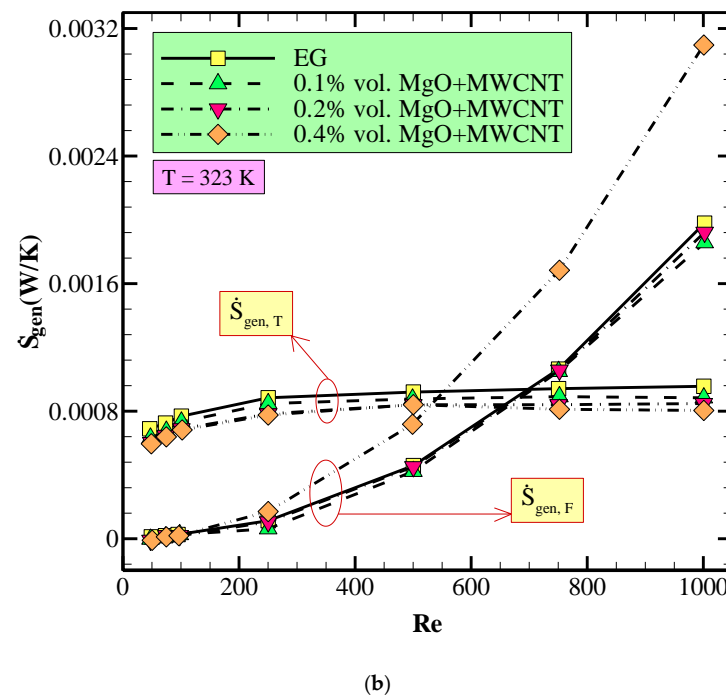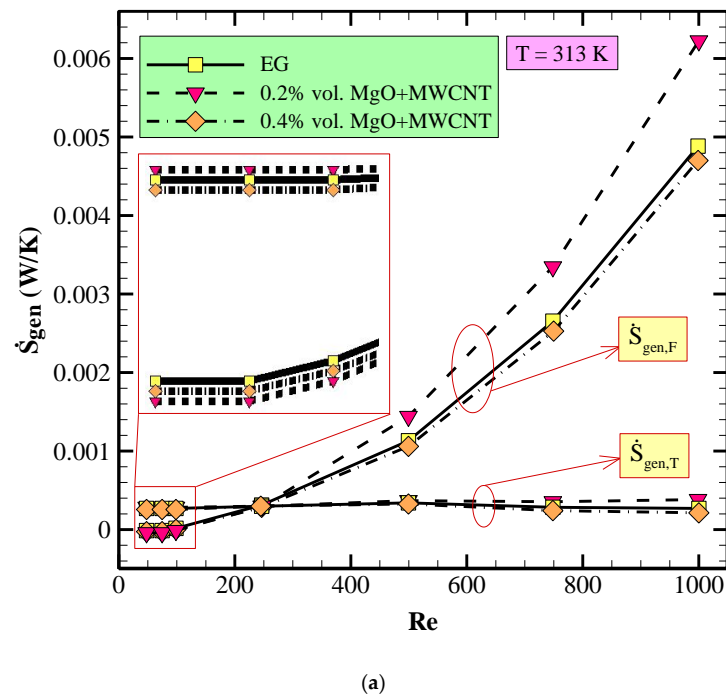
Figure 17. Effects of HNF with different VF on entropy generation for different Re and inlet temperatures (**a**) $T = 313$ K and (**b**) $T = 323$ K.

3.7. The Influence of Hybrid Nanofluid with Various Volume Fractions on Dimensionless Entropy at Various Re and Selected Inlet Temperature

Figure 18 illustrates the influence of the HNF with different VF on dimensionless entropy generation for various Reynolds numbers and inlet temperatures $T = 313$ K and $T = 323$ K. It is witnessed that the entropy generation reduces initially and then increases by increasing the fluid velocity (increasing the Reynolds number). This is because the entropy generation increases with HT and PD. For high fluid velocities (high Reynolds numbers) and inlet temperature of 313 K, HNF with a volume fraction of 0.2% is the most efficient case. Minimum dimensionless entropy generation corresponds to the HNF with volume fractions of 0.1% and 0.2% at inlet temperature 323 K. The results imply that the

EG/MgO-MWCNT HNF with a VF of 0.4% is introduced as the optimum case among all studied ones.

(**a**)

(**b**)
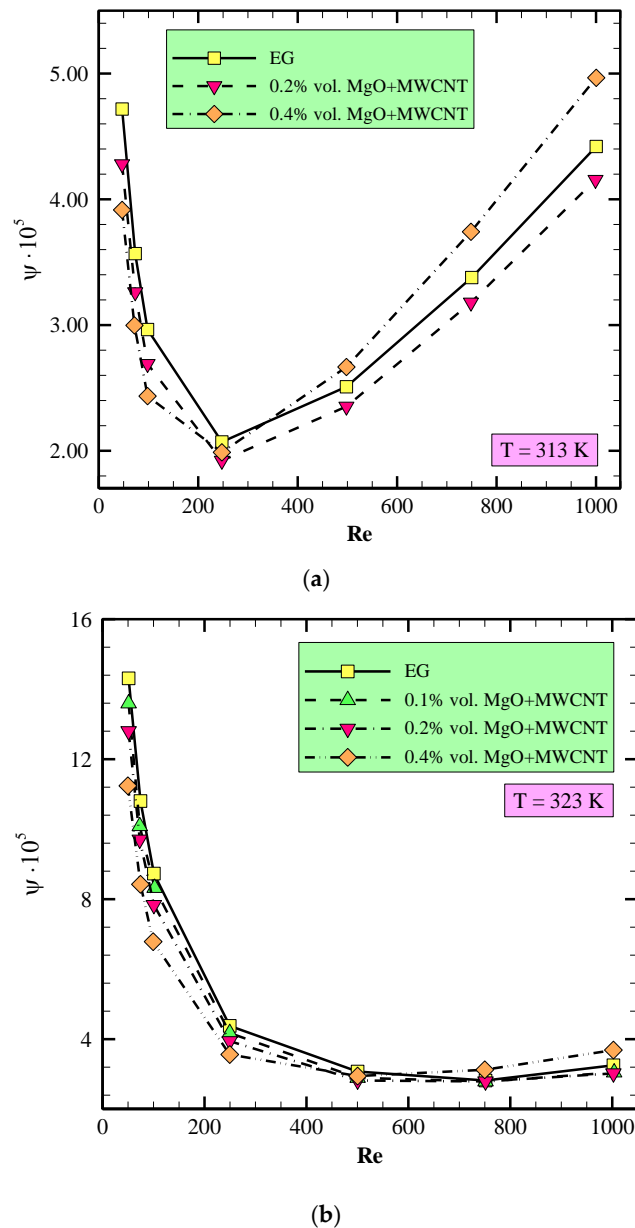
Figure 18. Effects of HNF with different VF on dimensionless entropy generation for different Re and inlet temperatures of (**a**) T = 313 K and (**b**) T = 323 K.

4. Conclusions

In this study, forced convection HT of a HNF in a heat exchanger with elliptical corrugated tubes was investigated. Three-dimensional (3D) multiphase governing equations were solved computationally using a control volume approach based on the SIMPLE algorithm. The range of Reynolds numbers 50 < Re < 1000 corresponds to laminar flow. Optimization was carried out by evaluation of various parameters to reach an optimal case with the maximum Nu and minimum PD and minimum entropy generation. The implications of the results achieved are summarized into the following six characteristics:

(i)   At T = 323K, the use of the EG/MgO-MWCNT NHF with a VF of 0.4% leads to higher Nu in comparison with the base fluid for all Re. However, at this temperature, the use of the EG/MgO-MWCNT HNF with a VF of 0.1% and 0.2% is more appropriate at very low Re.

(ii) As the Re increases, the pumping power increases. The value of pumping power for the EG/MgO-MWCNT HNF with a volume fraction of 0.4% is more than that for other cases at all Re.

(iii) Higher temperatures lead to larger PD. EG/MgO-MWCNT HNF with a volume fraction of 0.4% has less PD compared to the other HNF with a lower VF.

(iv) Thermal entropy generation reduces and frictional entropy generation increases with the VF of NPs and fluid velocity (Re).

(v) Since irreversible HT is the cause of increase in thermal entropy, the variations of $\dot{S}_{gen,T}$ are more important at lower Re.

(vi) The EG/MgO-MWCNT HNF with a VF of 0.4% is introduced as the optimum case among all studied ones.

In order to continue this study, the effect of different pipe cross-sections on the performance of the heat exchanger can be investigated. The effect of the presence of internal microfins in the pipes on thermal efficiency and also the effect of the type of nanofluid can be investigated.

Institutional Review Board Statement: Not applicable.

Informed Consent Statement: Not applicable.

Conflicts of Interest: The authors declare no conflict of interest.

Nomenclature

Symbols

c_P	Specific heat (J/kgK)
f	Friction factor
k	Thermal conductivity (W/mK)
P	Pressure (Pa)
T	Temperature (K)
V	Velocity

Greek Symbols

μ	Dynamic viscosity (mPa.s)
ρ	Density (m^3/kg)
η	Efficiency

Subscriptions

np	Nanoparticle
nf	Nanofluid

Abbreviations

HNF	Hybrid nanofluid
Re	Reynolds numbers
HE	Heat exchanger
Nu	Nusselt number
VF	Volume fraction
HT	Heat transfer
NFs	Nanofluids
PD	Pressure drop
NPs	Nanoparticles
f	Friction factor

References

1. Bhattacharyya, S.; Bashir, A.I.; Dey, K.; Sarkar, R. Effect of novel short-length wavy-tape turbulators on fluid flow and heat transfer: Experimental study. *J. Therm. Energy Gener. Transp. Storage Convers.* **2019**, *33*, 335–354. [CrossRef]
2. Bhattacharyya, S.; Chattopadhyay, H.; Pal, T.K.; Roy, A. Numerical investigation of thermohydraulics performance in elliptical twisted duct heat exchanger. *Lect. Notes Mech. Eng.* **2016**, 839–849. [CrossRef]
3. Bhattacharyya, S.; Chattopadhyay, H.; Benim, A.C. Simulation of heat transfer enhancement in tube flow with twisted tape insert. *Prog. Comput. Fluid Dyn.* **2017**, *17*, 193–197. [CrossRef]
4. Nadooshan, A.A.; Kalbasi, R.; Afrand, M. Perforated fins effect on the heat transfer rate from a circular tube by using wind tunnel: An experimental view. *Heat Mass Transf.* **2018**, *54*, 3047–3057. [CrossRef]
5. Gupta, M.; Singh, V.; Kumar, R.; Said, Z. A review on thermophysical properties of nanofluids and heat transfer applications. *Renew. Sustain. Energy Rev.* **2017**, *74*, 638–670. [CrossRef]
6. Bhattacharyya, S.; Vishwakarma, D.K.; Goel, V.; Chamoli, S.; Issakhov, A.; Meyer, J.P. Thermodynamics and heat transfer study of a circular tube embedded with novel perforated angular-cut alternate segmental baffles. *J. Therm. Anal. Calorim.* **2021**, *145*, 1445–1465. [CrossRef]
7. Bhattacharyya, S.; Saha, S.; Saha, S.K. Laminar flow heat transfer enhancement in a circular tube having integral transverse rib roughness and fitted with centre-cleared twisted-tape. *Exp. Therm. Fluid Sci.* **2013**, *44*, 727–735. [CrossRef]
8. Bhattacharyya, S.; Raghavendran, H.; Paul, A.R. The effect of circular hole spring tape on the turbulent heat transfer and entropy analysis in a heat exchanger tube: An experimental study. *Exp. Heat Transf.* **2020**, *34*, 493–512. [CrossRef]
9. Menni, Y.; Ghazvini, M.; Ameur, H.; Kim, M.; Ahmadi, M.H.; Sharifpur, M. Combination of baffling technique and high-thermal conductivity fluids to enhance the overall performances of solar channels. *Eng. Comput.* **2020**, *1*, 1–22. [CrossRef]
10. Osman, S.; Sharifpur, M.; Meyer, J.P. Experimental investigation of convection heat transfer in the transition flow regime of aluminium oxide-water nanofluids in a rectangular channel. *Int. J. Heat Mass Transf.* **2019**, *133*, 895–902. [CrossRef]
11. Menni, Y.; Ameur, H.; Sharifpur, M.; Ahmadi, M.H. Effects of in-line deflectors on the overall performance of a channel heat exchanger. *Eng. Appl. Comput. Fluid Mech.* **2021**, *15*, 512–529. [CrossRef]
12. Saifi, H.; Sari, M.R.; Kezzar, M.; Ghazvini, M.; Sharifpur, M.; Sadeghzadeh, M. Heat transfer through converging-diverging channels using Adomian decomposition method. *Eng. Appl. Comput. Fluid Mech.* **2020**, *14*, 1373–1384. [CrossRef]
13. Afrand, M.; Karimipour, A.; Nadooshan, A.A.; Akbari, M. The variations of heat transfer and slip velocity of FMWNT-water nano-fluid along the micro-channel in the lack and presence of a magnetic field. *Phys. E Low-Dimens. Syst. Nanostruct.* **2016**, *84*, 474–481. [CrossRef]
14. Singh, S.K.; Bhattacharyya, S.; Paul, A.R.; Sharifpur, M.; Meyer, J.P. Augmentation of heat transfer in a microtube and a wavy microchannel using hybrid nanofluid: A numerical investigation. *Math. Methods Appl. Sci.* **2020**. [CrossRef]
15. Vo, D.D.; Alsarraf, J.; Moradikazerouni, A.; Afrand, M.; Salehipour, H.; Qi, C. Numerical investigation of γ-AlOOH nano-fluid convection performance in a wavy channel considering various shapes of nanoadditives. *Powder Technol.* **2019**, *345*, 649–657. [CrossRef]
16. Yan, S.-R.; Kalbasi, R.; Karimipour, A.; Afrand, M. Improving the thermal conductivity of paraffin by incorporating MWCNTs nanoparticles. *J. Therm. Anal. Calorim.* **2020**, *145*, 2809–2816. [CrossRef]
17. Parsa, S.M.; Rahbar, A.; Koleini, M.H.; Javadi, Y.D.; Afrand, M.; Rostami, S.; Amidpour, M. First approach on nanofluid-based solar still in high altitude for water desalination and solar water disinfection (SODIS). *Desalination* **2020**, *491*, 114592. [CrossRef]
18. Giwa, S.O.; Sharifpur, M.; Ahmadi, M.H.; Murshed, S.M.S.; Meyer, J.P. Experimental investigation on stability, viscosity, and electrical conductivity of water-based hybrid nanofluid of MWCNT-Fe2O3. *Nanomaterials* **2021**, *11*, 136. [CrossRef]
19. Parsa, S.M.; Rahbar, A.; Javadi, Y.D.; Koleini, M.H.; Afrand, M.; Amidpour, M. Energy-matrices, exergy, economic, environmental, exergoeconomic, enviroeconomic, and heat transfer (6E/HT) analysis of two passive/active solar still water desalination nearly 4000m: Altitude concept. *J. Clean. Prod.* **2020**, *261*, 121243. [CrossRef]
20. Parsa, S.M.; Yazdani, A.; Dhahad, H.; Alawee, W.H.; Hesabi, S.; Norozpour, F.; Javadi, Y.D.; Ali, H.M.; Afrand, M. Effect of Ag, Au, TiO2 metallic/metal oxide nanoparticles in double-slope solar stills via thermodynamic and environmental analysis. *J. Clean. Prod.* **2021**, *311*, 127689. [CrossRef]

21. Parsa, S.M. Reliability of thermal desalination (solar stills) for water/wastewater treatment in light of COVID-19 (novel coronavirus "SARS-CoV-2") pandemic: What should consider? *Desalination* **2021**, *512*, 115106. [CrossRef]

22. Tian, X.X.; Kalbasi, R.; Jahanshahi, R.; Qi, C.; Huang, H.L.; Rostami, S. Competition between intermolecular forces of adhesion and cohesion in the presence of graphene nanoparticles: Investigation of graphene nanosheets/ethylene glycol surface tension. *J. Mol. Liq.* **2020**, *311*, 113329. [CrossRef]

23. Tshimanga, N.; Sharifpur, M.; Meyer, J.P. Experimental investigation and model development for thermal conductivity of glycerol–MgO nanofluids. *Heat Transf. Eng.* **2016**, *37*, 1538–1553. [CrossRef]

24. Rostami, S.; Kalbasi, R.; Talebkeikhah, M.; Goldanlou, A.S. Improving the thermal conductivity of ethylene glycol by addition of hybrid nano-materials containing multi-walled carbon nanotubes and titanium dioxide: Applicable for cooling and heating. *J. Therm. Anal. Calorim.* **2020**, *143*, 1701–1712. [CrossRef]

25. Wei, H.; Afrand, M.; Kalbasi, R.; Ali, H.M.; Heidarshenas, B.; Rostami, S. The effect of tungsten trioxide nanoparticles on the thermal conductivity of ethylene glycol under different sonication durations: An experimental examination. *Powder Technol.* **2020**, *374*, 462–469. [CrossRef]

26. Ibrahim, M.; Saeed, T.; Chu, Y.M.; Ali, H.M.; Cheraghian, G.; Kalbasi, R. Comprehensive study concerned graphene nano-sheets dispersed in ethylene glycol: Experimental study and theoretical prediction of thermal conductivity. *Powder Technol.* **2021**, *386*, 51–59. [CrossRef]

27. Parsa, S.M.; Rahbar, A.; Koleini, M.H.; Aberoumand, S.; Afrand, M.; Amidpour, M. A renewable energy-driven thermoelectric-utilized solar still with external condenser loaded by silver/nanofluid for simultaneously water disinfection and desalination. *Desalination* **2020**, *480*, 114354. [CrossRef]

28. Giwa, S.O.; Sharifpur, M.; Ahmadi, M.H.; Meyer, J.P. Magnetohydrodynamic convection behaviours of nanofluids in non-square enclosures: A comprehensive review. *Math. Methods Appl. Sci.* **2020**. [CrossRef]

29. Santra, S.; Sen, D.; Das, S.; Chakraborty, S. Electrohydrodynamic interaction between droplet pairs in a confined shear flow. *Phys. Fluids* **2019**, *31*, 032005. [CrossRef]

30. Li, X.; Gong, W.; Wang, H.; Li, T.; Attri, K.S.; Lewis, R.E.; Kalil, A.C.; Bhinderwala, F.; Powers, R.; Yin, G.; et al. O-GlcNAc transferase suppresses inflammation and necroptosis by targeting receptor-interacting serine/threonine-protein kinase 3. *Immunity* **2019**, *50*, 576–590. [CrossRef]

31. Buonomo, B.; Manca, O.; Bondareva, N.S.; Sheremet, M.A. Thermal and fluid dynamic behaviors of confined slot jets impinging on an isothermal moving surface with nanofluids. *Energies* **2019**, *12*, 2074. [CrossRef]

32. Mohammed, H.A.; Al-Shamani, A.N.; Sheriff, J.M. Thermal and hydraulic characteristics of turbulent nanofluids flow in a rib–groove channel. *Int. Commun. Heat Mass Transf.* **2012**, *39*, 1584–1594. [CrossRef]

33. Heidary, H.; Kermani, M.J.; Dabir, B. Influences of bipolar plate channel blockages on PEM fuel cell performances. *Energy Convers. Manag.* **2016**, *124*, 51–60. [CrossRef]

34. Ahmed, M.A.; Shuaib, N.H.; Yusoff, M.Z.; Al-Falahi, A.H. Numerical investigations of flow and heat transfer enhancement in a corrugated channel using nanofluid. *Int. Commun. Heat Mass Transf.* **2011**, *38*, 1368–1375. [CrossRef]

35. Ahmed, M.A.; Shuaib, N.H.; Yusoff, M.Z. Numerical investigations on the heat transfer enhancement in a wavy channel using nanofluid. *Int. J. Heat Mass Transf.* **2012**, *55*, 5891–5898. [CrossRef]

36. Ahmed, M.A.; Yusoff, M.Z.; Shuaib, N.H. Effects of geometrical parameters on the flow and heat transfer characteristics in trapezoidal-corrugated channel using nanofluid. *Int. Commun. Heat Mass Transf.* **2013**, *42*, 69–74. [CrossRef]

37. Arani, A.A.A.; Sadripour, S.; Kermani, S. Nanoparticle shape effects on thermal-hydraulic performance of boehmite alumina nanofluids in a sinusoidal–wavy mini-channel with phase shift and variable wavelength. *Int. J. Mech. Sci.* **2017**, *128–129*, 550–563. [CrossRef]

38. Sadripour, S.; Ghorashi, S.A.; Estajloo, M. Numerical investigation of a cavity equipped with corrugated heat source: A full convection-conduction-radiation coupling. *Am. J. Aerosp. Eng.* **2017**, *4*, 27–37. [CrossRef]

39. Hung, Y.M. Analytical study on forced convection of nanofluids with viscous dissipation in microchannels. *Heat Transf. Eng.* **2010**, *31*, 1184–1192. [CrossRef]

40. Torii, S.; Satou, Y.; Koito, Y. Experimental study on convective thermal-fluid flow transport phenomena in circular tube using nanofluids. *Int. J. Green Energy* **2010**, *7*, 289–299. [CrossRef]

41. Mohammed, H.A.; Bhaskaran, G.; Shuaib, N.H.; Abu-Mulaweh, H.I. Influence of nanofluids on parallel flow square microchannel heat exchanger performance. *Int. Commun. Heat Mass Transf.* **2011**, *38*, 1–9. [CrossRef]

42. Asha, S.K.; Deepa, C.K. Entropy generation for peristaltic blood flow of a magneto-micropolar fluid with thermal radiation in a tapered asymmetric channel. *Results Eng.* **2019**, *3*, 100024. [CrossRef]

43. Shi, X.; Wang, Y.; Huai, X.; Cheng, K. Influence of geometrical parameters on thermal-hydraulic performance and entropy generation in cross-wavy channels with variable air properties. *Appl. Therm. Eng.* **2019**, *157*, 113714. [CrossRef]

44. Gul, A.; Khan, I.; Makhanov, S.S. Entropy generation in a mixed convection Poiseulle flow of molybdenum disulphide Jeffrey nanofluid. *Results Phys.* **2018**, *9*, 947–954. [CrossRef]

45. Dormohammadi, R.; Farzaneh-Gord, M.; Ebrahimi-Moghadam, A.; Ahmadi, M.H. Heat transfer and entropy generation of the nanofluid flow inside sinusoidal wavy channels. *J. Mol. Liq.* **2018**, *269*, 229–240. [CrossRef]

46. Qian, X.; Yang, Y.; Lee, S.W. Design and evaluation of the lab-scale shell and tube heat exchanger (STHE) for poultry litter to energy production. *Processes* **2020**, *8*, 500. [CrossRef]

47. Ibrahim, H.; Sazali, N.; Shah, A.S.M.; Karim, M.S.A.; Aziz, F.; Salleh, W.N.W. A review on factors affecting heat transfer efficiency of nanofluids for application in plate heat exchanger. *J. Adv. Res. Fluid Mech. Therm. Sci.* **2019**, *60*, 144–154.
48. Qian, X.; Lee, S.W.; Yang, Y. Heat transfer coefficient estimation and performance evaluation of shell and tube heat exchanger using flue gas. *Processes* **2021**, *9*, 939. [CrossRef]
49. Nourollahi, M.; Farhadi, M.; Sedighi, K. Numerical study of mixed convection and entropy generation in the Poiseulle-Benard channel in different angles. *Therm. Sci.* **2010**, *14*, 329–340. [CrossRef]
50. Borgnakke, C.; Sonntag, R.E. *Fundamentals of Thermodynamics*, 7th ed.; Wiley: Hoboken, NJ, USA, 2009.
51. Bohne, D.; Fischer, S.; Obermeier, E. Thermal, conductivity, density, viscosity, and prandtl-numbers of ethylene glycol-water mixtures. *Ber. Der Bunsenges. Für Phys. Chem.* **1984**, *88*, 739–742. [CrossRef]
52. Yu, W.; France, D.M.; Smith, D.S.; Singh, D.; Timofeeva, E.V.; Routbort, J.L. Heat transfer to a silicon carbide/water nanofluid. *Int. J. Heat Mass Transf.* **2009**, *52*, 3606–3612. [CrossRef]
53. Launder, B.E.; Spalding, D.B. *Mathematical Models of Turbulence*; Academic Press: New York, NY, USA, 1972.
54. Patankar, S.V. *Numerical Heat Transfer and Fluid Flow*; Taylor & Francis Group: Abingdon, UK, 1980.
55. Anderson, J.D. *Computational Fluid Dynamics*; McGraw-Hill: New York, NY, USA, 1995.
56. Çengel, A.Y. *Heat Transfer—A Practical Approach*, 2nd ed. 2008. Available online: https://pdfroom.com/books/heat-transfer-a-practical-approach/3Jr2ExbgyvL (accessed on 20 February 2021).
57. Huminic, G.; Huminic, A. The influence of hybrid nanofluids on the performances of elliptical tube: Recent research and numerical study. *Int. J. Heat Mass Transf.* **2019**, *129*, 132–143. [CrossRef]